JOURNAL OF MATERIALS SCIENCE 13 (1978) 1680–1688

Fracture energy of epoxy resin under plane strain conditions

E. H. ANDREWS, A. STEVENSON
Department of Materials, Queen Mary College, Mile End Road, London, UK

The fracture behaviour of an epoxy resin has been studied by a method which involves the pressurization of an internal circular crack. The method can be used to study both cohesive fracture and the adhesive failure of an interface. Plane strain conditions are assured because the crack does not intersect a free surface and (for adhesive failure) shrinkage stresses are eliminated as a crack driving force. Using high speed photography, the dependence of crack speed on critical pressure and specimen geometry was determined. An elastic analysis permits the derivation of fracture energy as a function of crack velocity. Fracture energy values lay between 100 and 200 J m^{-3} at 35° C with a peak at a crack velocity of 37 m sec^{-1}.

1. Introduction

Fracture surface energies (denoted $\mathcal{T}$ in this paper $2\mathcal{T} \equiv \mathcal{G}_c$) have been measured for epoxy resins by several workers [1–4], and values between 100 and 10 000 J m^{-2} have been obtained. Andrews and King [5] found that $\mathcal{T}$ was a continuous function of crack growth rate through the glass transition temperature with a sharp peak below T_g at a crack speed of about 10^{-2} m sec^{-1}. Mai [4] found that fracture energy decreased with increasing crack speed in the range 10^{-4} to 10^{-2} m sec^{-1}; Young [6] and Selby and Miller [3] observed stick–slip behaviour in epoxy resins at certain temperatures which also indicates a sensitivity to crack speed. It is clear, therefore, that $\mathcal{T}$ for these materials is a rather variable quantity with a rate sensitivity somewhat greater than is normally encountered in glassy plastics (e.g. thermoplastics such as PMMA [7]).

All the experiments so far reported have been carried out on sheet material containing "through" cracks i.e., cracks whose fracture front intersects both major surfaces of the sheet. Williams [8] has pointed out that the measured fracture energy under these circumstances is an average of a plane stress value, operative at the free surfaces, and a plane strain value, operative in the centre of the sheet. Not only do plane strain and plane stress fracture energies differ, but their rate dependencies may also be quite different. Clearly, it would be desirable to obtain unequivocal plane strain values. Plane stress values, of course, can be obtained directly from very thin sheets.

One reason for our interest in epoxy resins is their application as adhesives. When we consider the failure of an adhesive joint between an epoxy resin and a rigid substrate (metal, glass etc.) a further uncertainty arises. Stresses are set up in the system due to differential thermal contraction between the adhesive and the substrate and, if the fracture front intersects free surfaces, these stresses tend to drive crack propagation at or near the interface.

The fracture test described in this paper was designed to overcome the problems referred to. That is, it was designed to provide an unequivocal plane strain value for the fracture energy and also to eliminate contraction stress as a driving force in adhesive failure tests.

In this paper we describe the test and the experimental apparatus. An elastic analysis is also outlined which permits the fracture energy $\mathcal{T}$ to be derived from the critical pressure for crack growth and the specimen geometry. The theoretical analysis is shown to be valid experimentally and used to

derive $\mathcal{T}$ as a function of crack velocity for a particular epoxy resin at room temperature.

2. Experimental

2.1. Basic design of test

The test is an extension of that proposed by Dannenberg [9] and by Williams [10] for thin flexible films adhering to rigid substrates (the "blister test"). A flat circular "crack" is created either at an interface or internal to the solid to be tested, and fluid pressure is applied to the crack until it propagates. In the present test the solid is not required to be flexible and its thickness is unlimited. The two basic configurations are shown in Figs. 1a and b and refer respectively to adhesive and cohesive failure tests. The symmetry about the axis A–A is circular in all cases.

The initial circular crack is created by use of a circular disc of PTFE, 2.5×10^{-4} m in thickness. The disc may be positioned at the interface between the brass base block (B in Fig. 1a) or elevated by means of a metal collar (C in Fig. 1b) to provide an internal flaw. When studying epoxy resins, the resin is simply poured into an open-top mould formed around the brass block by a cylinder of PTFE film, care being taken not to dislodge the PTFE disc. The resin is then oven-cured in the normal way.

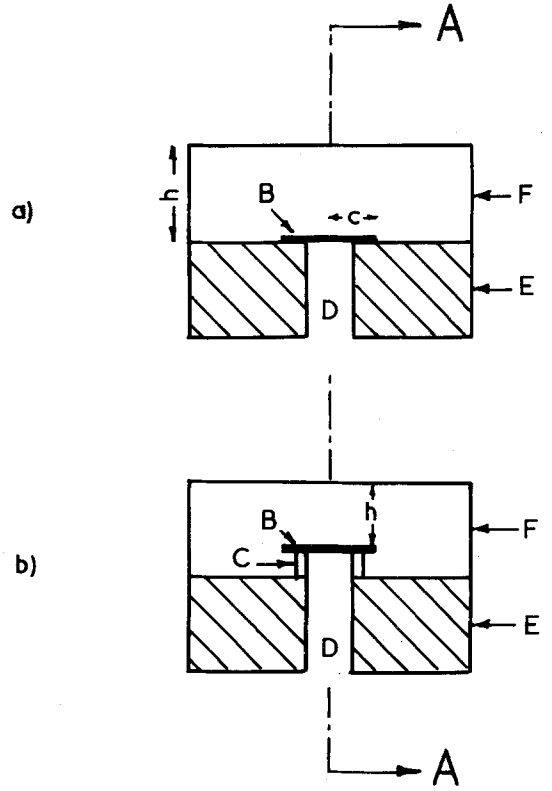

Figure 1 (a) Adhesive and (b) Cohesive test specimens, with circular symmetry about axis A–A; B is PTFE disc (thickness exaggerated); C is elevation collar used for cohesive mode tests; D is pressurization orifice; E is brass base block; F is cast resin. Specimen dimensions are crack radius, c, and thickness, h.

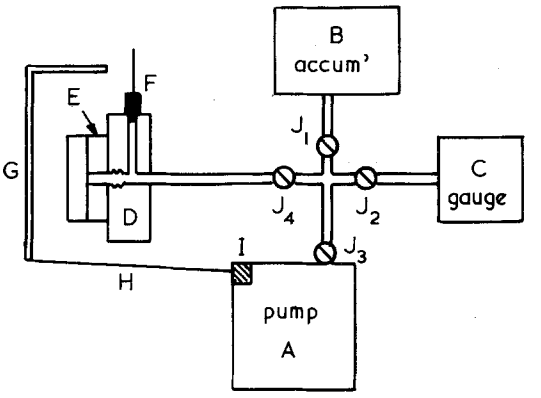

Figure 2 Schematic diagram of experimental apparatus. A, pump; B, nitrogen accumulator; C, bourdon gauge; D, test head; E, specimen base block; F, high speed pressure transducer; G, glass fronted test cell; H, catch tray; I, oil filter; J, control valves.

2.2. Pressurization equipment

The circular crack is internally pressurized via the orifice (D in Fig. 1) by means of the system shown schematically in Fig. 2. The system is oil-filled except for a bubble of air trapped in the orifice D which thus acts as the pressurizing fluid in contact with the specimen. Alternatively the air can be replaced by a test environment such as water to study the effects of environmental attack.

Pressure build-up is provided by a piston pump (by Marshalsea Hydraulics Ltd.) denoted A in Fig. 2 giving pressurization rates from 10 to 10^6 p.s.i. sec^{-1} up to a maximum pressure of 10^4 p.s.i. The pressure is stabilized by a nitrogen filled pressure accumulator (B) and recorded on a Bourdon dial gauge (C). High pressure tubing leads to the test-head (D) to which the brass base block of the specimen (E) can be screwed. The test head incorporates a thin film pressure transducer (F) connected to a u.v. chart recorder capable of response in the 1 to 10 m sec time range. Fig. 3a shows the importance of the accumulator in damping out unwanted pressure oscillations at low rates of pressurization, and Fig. 3b shows a typical pressure–time graph.

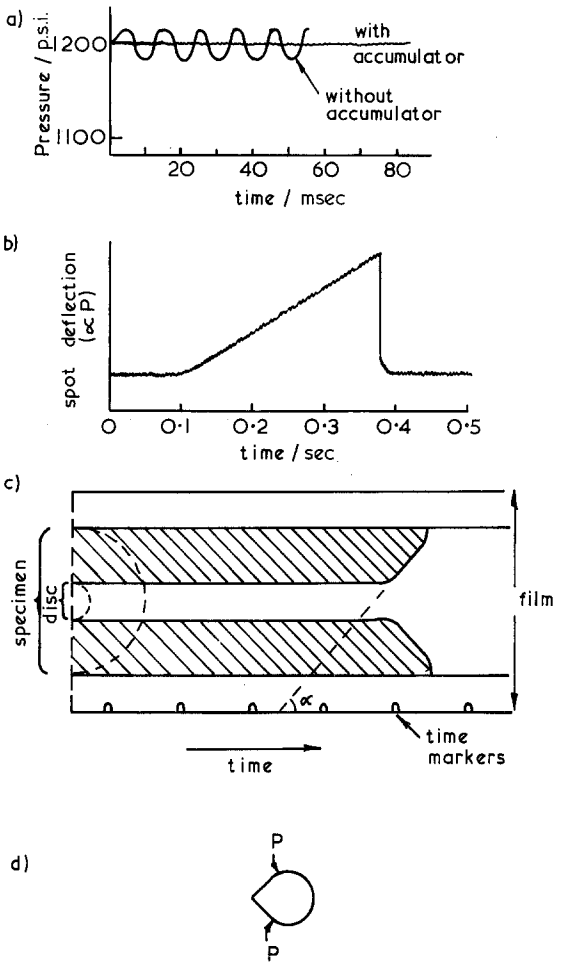

Figure 3 (a) Smoothing of pressure fluctuations by use of accumulator. (b) A typical u.v. recorder trace. (c) Streak photograph of fracture event (sketch). (d) Shape of PTFE discs. Fracture initiates at points P.

A glass-fronted test cell (G) protects the operator and the environment from oil and debris when the specimen breaks, and the spilt oil is returned to the pump reservoir via a catch tray (H) and filter (I).

Pressurization rates are adjusted by means of control valves (J) which can be set to provide any desired rate of pressure build-up. Maximum pressurization rate is obtained, using the accumulator as a presssure source, by throwing open valves J_1 and J_4.

2.3. Crack velocity measurement

The measurement of crack-velocity is carried out using high speed photography relying, of course, on the transparency of the epoxy resin. (For opaque materials, an electrical resistance method has been envisaged but not yet developed). The apparatus employed is a rotating prism camera (by J. Hadland (PI) Ltd.) capable of a framing speed of 11 000 frames per second. For the most part, however, the camera was used in a streak mode at a film translation speed of $7.7\,\mathrm{m\,sec^{-1}}$ which provided a continuous record of crack velocities up to about $400\,\mathrm{m\,sec^{-1}}$.

Lighting was non-coherent and supplied by tungsten halogen lamps set at a variety of angles to the specimen.

The photographic record obtained was a plan view of the circular crack smeared along the direction of travel of the film. A typical record is shown in Fig. 3c.

A problem arises at this stage because, with circular symmetry, the crack cannot be guaranteed to grow equally along all radii. The streak record, of course, only reveals growth in a direction perpendicular to the direction of image smearing. It was found possible to alleviate this difficulty by cutting the PTFE discs with two "flats" as shown in Fig. 3d. Framing photography shows that crack propagation from such a disc always occurs first near the point P, and this allows the specimen to be oriented relative to the camera in such a way that initial growth is always perpendicular to the smearing direciton.

The crack velocity $\dot{c}$ is obtained from Fig. 3c by measuring the angle α, whence

$$\dot{c} = V \tan \alpha \qquad (1)$$

where V is the image translation speed (film speed divided by the magnification).

2.4. Materials

The epoxy resin used was a diglycidyl ether of bisphenol A of molecular mass ~ 370 (Shell Epikote 828). The hardener was a blend of two cycloaliphatic amines with added benzyl alcohol as an accelerator (Shell Epikure 114). After outgassing under vacuum at 60 to 70° C the components were mixed in the stoichiometric ratio of 5 parts resin to 2 parts hardener.

After casting, specimens were left to gel for 24 hours at room temperature and postcured at 130° C for 1.5 h. This procedure was shown, by thermal analysis, to give maximum cross-linking (maximum glass transition temperature). Final cooling was carried out slowly at 0.5° C per minute.

The geometrical variables investigated were flaw radius, c, and specimen thickness, h, measured above the flaw (see Fig. 1). Values were:

$$c = 0.575, 0.65, 0.75, 0.85 \text{ cm}$$

$$h = 0.2, 0.4, 0.7, 1.0, 1.5 \text{ cm}$$

All tests were carried out at $35 \pm 5^\circ$ C, using the arrangement of Fig. 1b. The relatively high temperature resulted from the lighting units.

3. Analysis

The energy release available for crack propagation in a specimen such as used here can be regarded as coming from two superimposed elastic stress fields. The "near field" is the stress field set up around an internal crack in an infinite medium and superimposed upon this is the "far field" due to gross deflection of the specimen as a whole. In the case of our specimens, the "far field" involves the plate-like deflection of the material above the artificial crack, as shown in Fig. 4.

If the specimen is infinitely thick ($h \to \infty$), the "far field" energy will tend to zero because the plate is too thick to bend or deflect. Under these circumstances a Griffith type analysis is in order, such as given by Sneddon [11, 12] for a penny-shaped crack subject to internal pressurization.

Sneddon gives,

$$\mathscr{E}_n = \frac{8(1-\nu^2)}{3E} P^2 c^3 \qquad (2)$$

where $\mathscr{E}_n$ is the energy stored in the "near field". If the penny-shaped flaw is raised from the substrate as in our Fig. 1b. we shall assume $\mathscr{E}_n$ to be given by Sneddon's formula. When the crack is located at the interface with a rigid substrate (Fig. 1a), we shall take $\mathscr{E}_n$ as *half* the value given in Equation 2. Clearly a general case is given by

$$\mathscr{E}_n = \frac{\alpha 8(1-\nu^2)}{3E} P^2 c^3 \qquad (3)$$

where $0.5 \leqslant \alpha \leqslant 1$.

The strain energy of the "far field" can be calculated by the method of Timoshenko and Goodier [13]. Their solution for the stresses in a deflected thick shell (Fig. 4) is:

$$\sigma_r = -\frac{6P}{h^3}\left(r^2 Z - \frac{2Z^3}{3}\right)$$

$$\sigma_z = -\frac{6P}{h^3}\left\{\frac{1}{3}Z^3 - \left(\frac{h}{2}\right)^2 Z + \frac{2}{3}\left(\frac{h}{2}\right)^3\right\}$$

$$\tau_{rz} = -\frac{6P}{h^3}\left\{\left(\frac{h}{2}\right)^2 - Z^2\right\} \qquad (4)$$

where P is the internal pressure, σ_r, σ_z are the radial and vertical direct stresses and τ_{rz} the shear stress in the plane of the sheet.

This leads [13] to the following expression for the deflection, ω, of the "deflection surface" i.e. the median plane of the thick shell.

$$\omega = \frac{P}{64D}\left\{(c^2 - r^2)^2 + \frac{4h^2}{(1-\nu)}(c^2 - r^2)\right\} \qquad (5)$$

where $D = Eh^3/12(1-\nu^2)$, is the plate flexural rigidity.

The elastic energy stored by the applied stress, acting through the equilibrium displacement ω, is

$$\mathscr{E}_f = \frac{1}{2}\int_0^{2\pi}\int_0^c \omega P r \, dr \, d\theta \qquad (6)$$

which, from Equation 5, yields,

$$\mathscr{E}_f = \frac{P^2\pi(1-\nu^2)}{32Eh^3}\left\{c^6 + \frac{6h^2}{1-\nu} c^4\right\} \qquad (7)$$

Just as Sneddon used the "near field" elastic energy to calculate an energy release rate for an infinite system, so Williams [10] used a simplified form of the "far field" energy $\mathscr{E}_f$ to obtain the energy release rate for a thin plate (the "blister test"). Williams assumed $h \ll c$ so that only the term in c^6 (Equation 7) appears in his calculations.

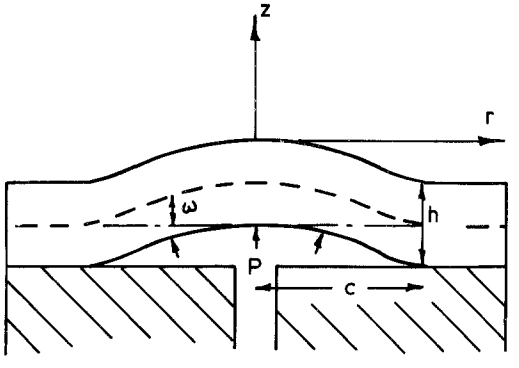

Figrue 4 Analysis of the "far field". Specimen above the crack undergoes plate-like deflection, ω. The broken line shows the "deflection surface".

Clearly however, the full story is obtained only when both $\mathscr{E}_f$ and $\mathscr{E}_n$ are considered together. We have therefore the total elastic energy,

$$\mathscr{E} = \mathscr{E}_n + \mathscr{E}_f \tag{8}$$

so that the energy release rate becomes, at constant deflection,

$$-\left.\frac{d\mathscr{E}}{dA}\right|_\omega = -\left.\frac{1}{2\pi c}\frac{d\mathscr{E}}{dc}\right|_\omega = \left.\frac{1}{2\pi c}\frac{d\mathscr{E}}{dc}\right|_P \tag{9}$$

Note that, as in the case of constant load on a sheet specimen, the energy release rate is the negative of the total change of energy at constant pressure. The energy stored in the specimen *increases* as the crack grows at constant pressure, but decreases at constant deflection. Thus since $\mathscr{E} = \mathscr{E}_n + \mathscr{E}_f$,

$$-\left.\frac{d\mathscr{E}}{dA}\right|_\omega = \frac{P^2c}{E}(1-\nu^2)\left[\frac{3}{32}\left[\left(\frac{c}{h}\right)^3 + \left(\frac{c}{h}\right)\frac{4}{1-\nu}\right] + \frac{1}{\pi}\right] \tag{10}$$

At the critical pressure for crack propagation, $P = P_c$ and the critical energy release rate equals $2\mathscr{T}$ (two surfaces), where $\mathscr{T}$ is the fracture energy as defined elsewhere [14]. Thus

$$\frac{P_c^2 c}{E} = 2\mathscr{T} f_1\left(\frac{h}{c}\right) \tag{11}$$

$$f_1(h/c) = \frac{1}{1-\nu^2}\left[\frac{3}{32}\left[\left(\frac{c}{h}\right)^3 + \left(\frac{c}{h}\right)\frac{4}{1-\nu}\right] + \frac{1}{\pi}\right]^{-1} \tag{12}$$

Equation 12 applies to the case shown in Fig. 1b. For the interfacial crack location,

$$f_2(h/c) = \frac{1}{1-\nu^2}\left[\frac{3}{32}\left[\left(\frac{c}{h}\right)^3 + \left(\frac{c}{h}\right)\frac{4}{1-\nu}\right] + \frac{2}{\pi}\right]^{-1} \tag{13}$$

Plots of f_1 and f_2 against (h/c) are given in Fig. 5 together with the Williams approximation for very thin sheets and the Sneddon limit for infinite specimens. As we shall see, most of the data from experimentally tractable specimens falls between the limits of applicability of the limiting cases and required the full solution given here.

4. Results and discussion

Specimen fracture resulted in the expulsion of a truncated cone making an angle γ with the plane of the disc. The cone angle depended on the specimen thickness and has to be known in order to correct the apparent crack velocity obtained photographically. The camera gives a plan view of the fracture event and the linear crack speed is actually larger by a factor of $(\cos\gamma)^{-1}$ than the apparent velocity. This correction has been applied in all data reported below.

Peak pressures, P_c, which are also the critical pressures for crack growth, were recorded for a range of pressurization rates and specimen geometries. Simultaneous determinations were made of initial crack velocity.

In accordance with the analytical approach given in Section 3, the data have been plotted first of all in terms of the parameter $P_c^2 c/E$ versus crack velocity $\dot{c}$. These data are shown in Figs. 6, 7 and

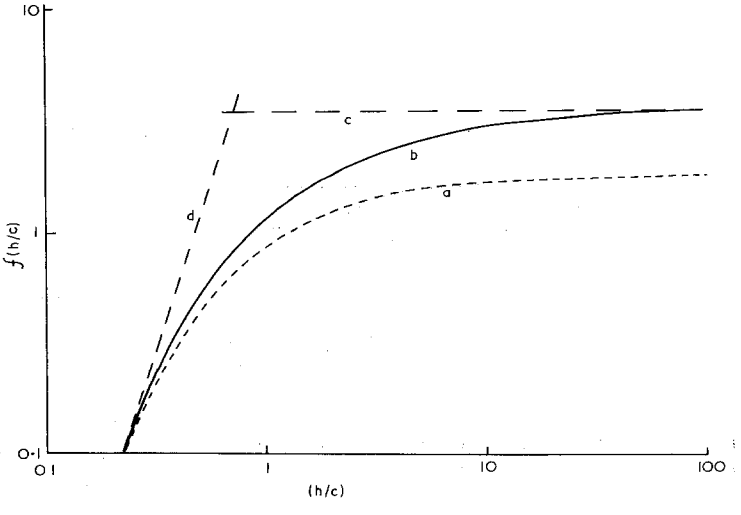

Figure 5 The function $f(h/c)$: (a) adhesive case $f_2(h/c)$; (b) cohesive case $f_1(h/c)$; (c) Sneddon limit; (d) Williams limit.

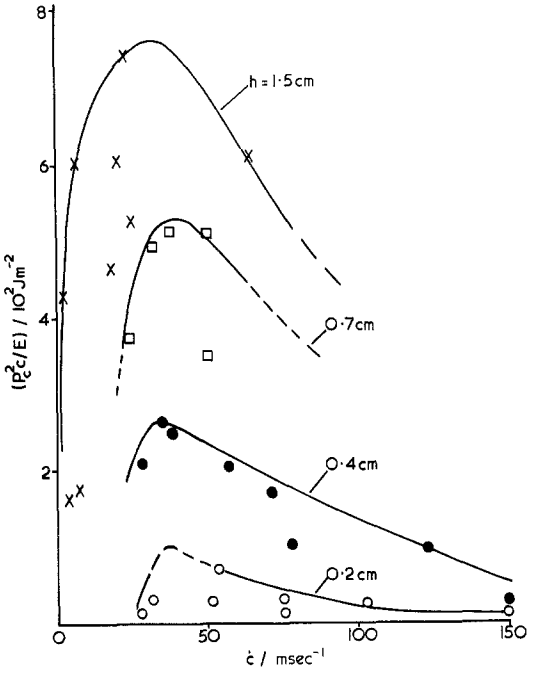

Figure 6 The parameter $(P_c^2 c/E)$ as a function of crack velocity for a crack radius $c = 0.575$ cm. Curves represent maximum envelope to data.

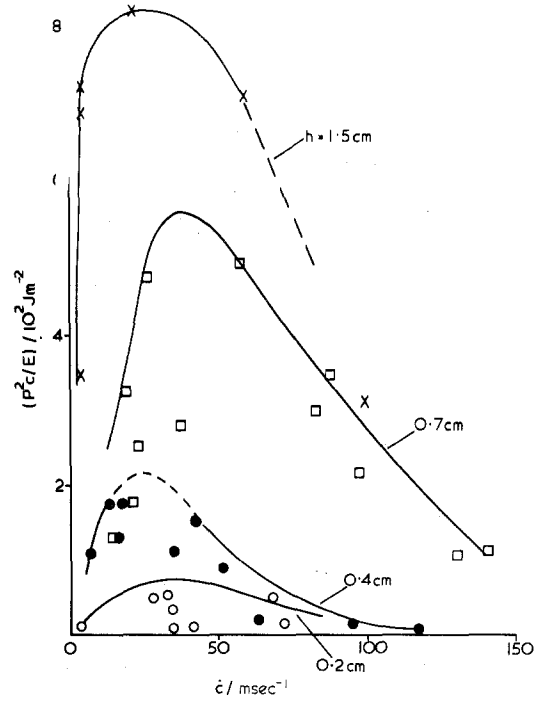

Figure 7 As Fig. 6 but for $c = 0.75$ cm.

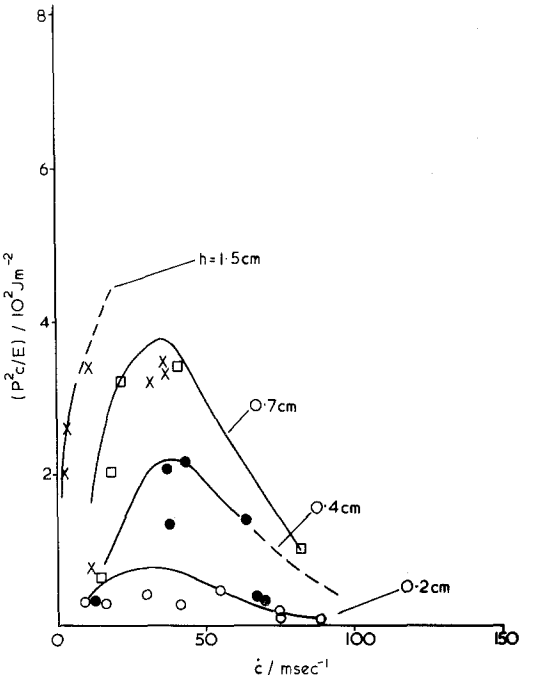

Figure 8 As Fig. 6 but for $c = 0.85$ cm.

8, each figure giving results for one value of crack radius and three values of specimen thickness, h. It is clear that the pressure for fracture is strongly dependent on both the parameter h and the velocity of crack growth, showing a consistent maximum at $\dot{c} \sim 35\,\mathrm{m\,sec^{-1}}$.

Data points show considerable scatter and this was eventually traced to imperfections in the PTFE discs. The kind of imperfection is shown in Fig. 9 and gives rise to a sharper-than-normal crack tip. In order to standardize the results, the curves of Figs. 6 to 8 have been drawn through the *maximum* $P_c^2 c/E$ values since these should correspond to unflawed discs. It is clear, of course, that crack tip sharpness is a variable of some importance which was not strictly under control in the experiments reported here. It also follows that the results

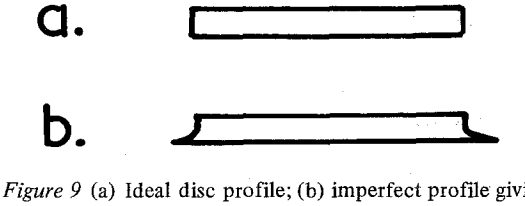

Figure 9 (a) Ideal disc profile; (b) imperfect profile giving rise to sharp crack tips and low critical pressures for fracture. Disc thickness exaggerated.

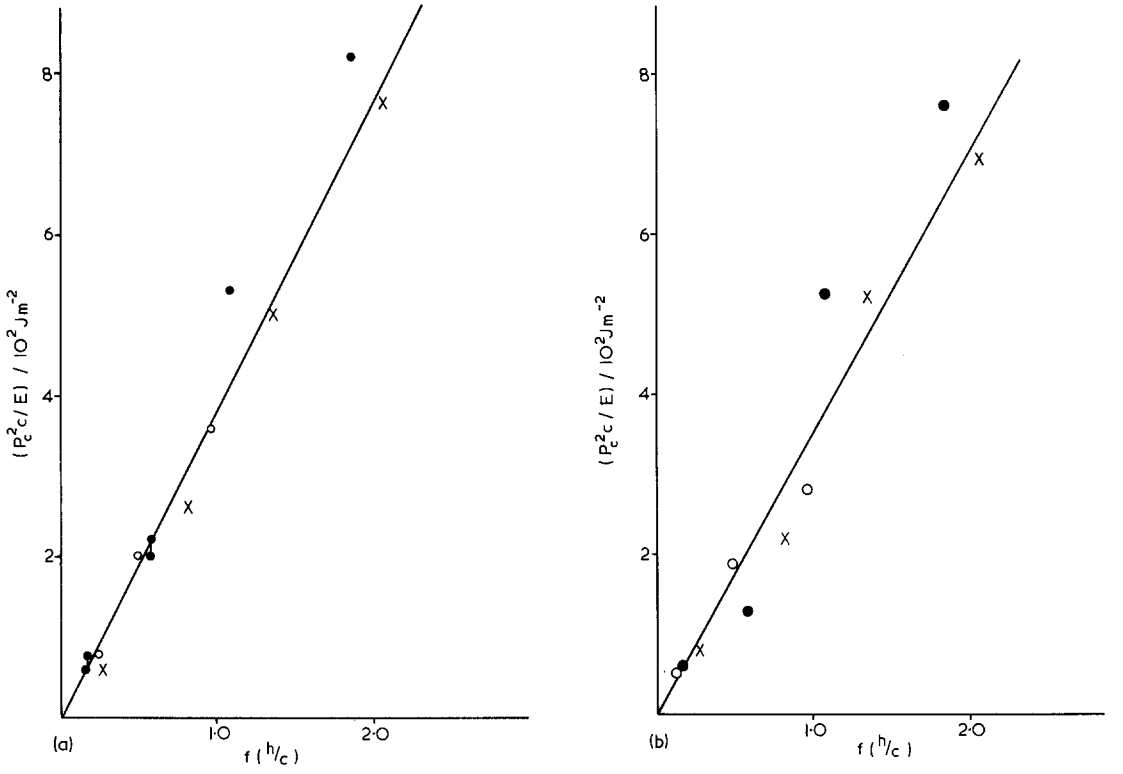

Figure 10 Typical plots of the parameter $(P_c^2 c/E)$ as a function of $f_1(h/c)$. All values of c, h define a single straight line for each velocity of slope $2\mathcal{T}$. (a) At 30 m sec^{-1}; (b) at 50 m sec^{-1}.

will be dependent on disc thickness and that "fracture energy" as determined here is a function of crack tip radius. This appears to be a consistent feature of materials displaying plastic flow.

The analysis of Section 3 gives

$$\frac{P_c^2 c}{E} = f_1(h/c)\, 2\mathcal{T}(\dot{c}) \qquad (11)$$

where $f_1(h/c)$ is given by Equation 12. A plot of $(P_c^2 c/E)$ against $f_1(h/c)$ at constant crack velocity should give a single straight line for all (c, h) having a slope equal to twice the fracture energy $2\mathcal{T}(\dot{c})$ of the solid.

Plots of $(P_c^2 c/E)$ against $f_1(h/c)$, using the smoothed data of Figs. 6 to 8, are given in Fig. 10 for two selected velocities, 30 and 50 m sec^{-1}. They reveal excellent agreement with theory, as do plots at other velocities.

Finally, from the slopes of such curves as shown in Fig. 10 the dependence of fracture energy upon velocity can be derived and is shown in Fig. 11 spanning more than two decades of $\dot{c}$. There is a smooth dependence of $2\mathcal{T}$ upon $\dot{c}$ with a clearly defined maximum at 37 m sec^{-1}; $2\mathcal{T}$ varies between 40 J m^{-2} at the lowest rates measured and 400 J m^{-2} at the peak. It is interesting to note that King and Andrews [15] have obtained a lower theoretical limit to $2\mathcal{T}$ (for the same epoxy resins used in this study) of around 3 J m^{-2}. This value would apply to a situation where no energy losses occurred i.e. to perfectly elastic conditions. Although the lowest measured

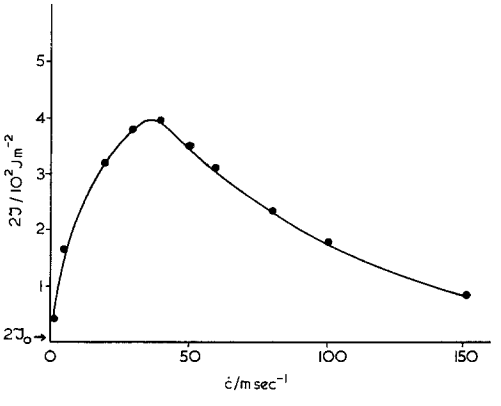

Figure 11 Fracture energy dependence upon crack velocity at 35 ± 5° C. Epoxy resin under plane strain.

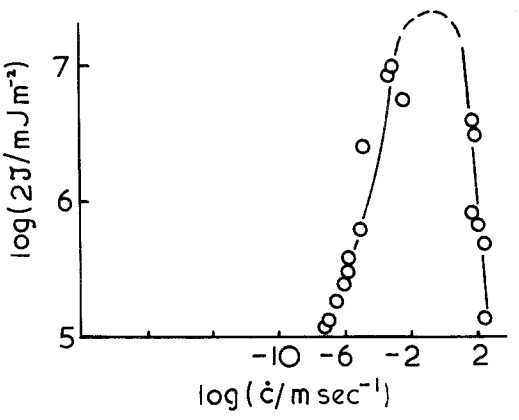

Figure 12 Fracture energy dependence upon crack velocity for sheet specimens of epoxy resin (same material as Fig. 11) at temperatures between 20 and 86° C. Mixed plane stress–plane strain conditions (after [5]).

value in these experiments is still an order of magnitude larger than this limiting value, the curve of Fig. 11 can be extrapolated with ease to such a value at $\dot{c} = 0$, as shown.

This, of course, only applies to the present test in which plain strain conditions apply absolutely. In other work on sheet specimens [4], admittedly on different epoxy resin systems, $2\mathscr{T}$ appears to *increase* over the range 150 to 300 J m^{-2} as the velocity tends towards zero. This could be due to a decrease in yield stress with increasing time giving larger and larger plane-stress plastic zones at the free surfaces as $\dot{c}$ diminishes. It could also however, be due to different rate effects in different epoxy resins.

A further point of comparison arises with King's data [5] for edge crack specimens of the same epoxy resin, shown in Fig. 12. The peak in $\mathscr{T}$ occurs somewhere between crack speeds of 10^2 and 10^{-2} m sec^{-1} and is thus compatible with the present data in this respect. The absolute magnitude of $2\mathscr{T}$, however, is 10^4 J m^{-2} for the 3 mm thick sheet specimens at the peak, compared with 400 J m^{-2} in the plain strain measurements reported here. The factor of 25 between these two measurements emphasises the large potential effect of plane-stress deformations in sheet specimens.

5. Conclusion

The fracture energy $\mathscr{T}$ of an epoxy resin measured in plane strain is up to 25 times smaller than that of the same material measured on sheet specimens where plane-stress surface deformations can occur. The dependence of $\mathscr{T}$ upon crack velocity in the range $1 \ll \dot{c} \ll 150$ m sec^{-1} is qualitatively similar to that in sheet specimens, with a peak at 37 m sec^{-1}. Under plane strain conditions it appears possible to extrapolate the curve of $\mathscr{T}$ against $\dot{c}$ to the theoretical minimum value of $\mathscr{T}$ at $\dot{c} = 0$.

This strongly suggests that the rise of $\mathscr{T}$ with $\dot{c}$ to the left of the peak is a viscoelastic phenomenon, and this is supported by King's data [5] which shows that this part of the curve is continuous through the glass transition temperature, i.e. the glassy state data are continuous with the rubber-like state data which are unquestionably viscoelastic in character.

The decrease in $\mathscr{T}$ with crack speed above 37 m sec^{-1} then appears to be a consequence of a rate dependent yield stress which increasingly limits the extent of plastic flow as velocity increases.

In work to be published later, there is a strong suggestion that the fracture energy begins to increase again at crack speeds above about 150 m sec^{-1}. This may be due to the onset of significant inertia effects at these high speeds.

There remains, of course, the uncertain effect of crack tip bluntness. Since a blunt crack provides added scope for local plasticity it is possible that the rate dependence observed in this work, and exhibited in Fig. 11, is determined in part by the crack tip radius and is not intrinsic to a plane strain situation.

On the other hand, of course, no crack tip can be infinitely sharp, especially in an amorphous glass close to its glass transition temperature. By its very nature, therefore, the phenomenon of plane strain fracture in such materials needs to be studied as a function of crack tip radius. Only then will the material behaviour be fully defined.

Acknowledgement

Thanks are due to the Science Research Council for their support of this research.

References

1. L. J. BROUTMAN and F. J. McGARRY, *J. Appl. Polymer Sci.* 9 (1965) 589.
2. W. D. BASCOM and R. L. COTTINGTON, *J. Adhesion* 7 (1976) 333.
3. K. SELBY and L. E. MILLER, *J. Mater. Sci.* **10** (1975) 12.
4. Y. W. MAI and A. G. ATKINS, *ibid.* **10** (1975) 2000.
5. E. H. ANDREWS and N. E. KING, *ibid.* (in press).
6. R. J. YOUNG and S. YAMINI, *Polymer* **18** (1977) 1075.

7. G. P. MARSHALL, L. E. CULVER and J. G. WILLIAMS, *Int. J. Fracture* 9 (1973) 295.
8. E. PLATI and J. G. WILLIAMS, *Polymer* 16 (1975) 915.
9. H. DANNENBERG, *J. Appl. Polymer Sci.* 14 (1961) 125.
10. M. L. WILLIAMS, *Int. J. Fracture* 10 (1974) 33.
11. I. N. SNEDDON, *Proc. Roy. Soc. (Lond.) A* 187 (1946) 229.
12. *Idem,* "Crack problems in the Classical Theory of Elasticity" (John Wily & Sons, New York, 1969).
13. S. TIMOSHENKO and J. GOODIER, "Theory of Elasticity" (McGraw–Hill, New York, 1954).
14. E. H. ANDREWS and N. E. KING, *J. Mater. Sci.* 11 (1976) 2004.
15. N. E. KING and E. H. ANDREWS, *ibid.* 13 (1978) 1291.

Received 30 September and accepted 13 December 1977.